



LJMU Research Online

Matthews, TR, Hodgkins, R, Guðmundsson, S, Pálsson, F and Björnsson, H

Inter-decadal variability in potential glacier surface melt energy at Vestari Hagafellsjökull (Langjökull, Iceland) and the role of synoptic circulation

<http://researchonline.ljmu.ac.uk/id/eprint/1531/>

Article

Citation (please note it is advisable to refer to the publisher's version if you intend to cite from this work)

Matthews, TR, Hodgkins, R, Guðmundsson, S, Pálsson, F and Björnsson, H (2014) Inter-decadal variability in potential glacier surface melt energy at Vestari Hagafellsjökull (Langjökull, Iceland) and the role of synoptic circulation. International Journal of Climatology. ISSN 1097-0088

LJMU has developed **LJMU Research Online** for users to access the research output of the University more effectively. Copyright © and Moral Rights for the papers on this site are retained by the individual authors and/or other copyright owners. Users may download and/or print one copy of any article(s) in LJMU Research Online to facilitate their private study or for non-commercial research. You may not engage in further distribution of the material or use it for any profit-making activities or any commercial gain.

The version presented here may differ from the published version or from the version of the record. Please see the repository URL above for details on accessing the published version and note that access may require a subscription.

For more information please contact researchonline@ljmu.ac.uk

<http://researchonline.ljmu.ac.uk/>

Inter-decadal variability in potential glacier surface melt energy at Vestari Hagafellsjökull (Langjökull, Iceland) and the role of synoptic circulation

Journal:	<i>International Journal of Climatology</i>
Manuscript ID:	Draft
Wiley - Manuscript type:	Research Article
Date Submitted by the Author:	n/a
Complete List of Authors:	Matthews, Tom; National University of Ireland, Geography Hodgkins, Richard; Loughborough University, Geography Guðmundsson, Sverrir; University of Iceland, Institute of Earth Sciences Pálsson, Finnur; University of Iceland, Institute of Earth Sciences Björnsson, Helgi; University of Iceland, Institute of Earth Sciences
Keywords:	Glacier melt modelling, Glacier surface energy balance, Synoptic circulation, North Atlantic Oscillation, Greenland Blocking Index

Melt energy and synoptic circulation at Vestari Hagafellsjökull

1
2
3
4 1 Inter-decadal variability in potential glacier surface melt energy at
5
6
7 2 Vestari Hagafellsjökull (Langjökull, Iceland) and the role of
8
9
10 3 synoptic circulation
11
12

13
14 4 Matthews¹ T, Hodgkins² R, Guðmundsson³ S, Pálsson³ F, Björnsson³ H
15
16
17
18

19 6 ¹Department of Geography, National University of Ireland, Maynooth
20

21 7 ²Department of Geography, Loughborough University, UK
22

23 8 ³Institute of Earth Science, University of Iceland, Iceland
24
25
26
27

28
29 10 **Corresponding author:**
30

31 11 Tom Matthews
32

33 12 Department of Geography
34

35
36 13 National University of Ireland
37

38 14 Maynooth
39

40 15 Kildare
41

42 16 Republic of Ireland
43
44

45
46 17 e-mail: tom.matthews@nuim.ie
47
48

49 18
50

51 19
52

53 20 **Key words:** Glacier melt modelling; Glacier surface energy balance; Synoptic circulation;
54

55 21 North Atlantic Oscillation; Greenland Blocking Index
56
57
58
59
60

Melt energy and synoptic circulation at Vestari Hagafellsjökull

1
2
3 23

Abstract

4
5
6
7 24 The Surface Energy Balance (SEB) of glaciers, although of considerable importance for
8
9 25 understanding the melt response to climate change, is generally analysed only for brief time
10
11 26 periods due to the logistical challenges of meteorological measurement campaigns on
12
13 27 glaciers. Insight into low-frequency changes in the SEB in response to climate warming and
14
15 28 variable atmospheric circulation patterns has thus been limited. Here this problem is
16
17 29 addressed by using ERA-Interim reanalysis data to extend glacier-meteorological records at
18
19 30 two locations on Vestari Hagafellsjökull for the period 1979-2012. Trend analysis is
20
21 31 conducted for this series before the role of synoptic circulation in modulating surface
22
23 32 energetics is investigated. The results indicate that potential melt energy has increased
24
25 33 significantly throughout the period of simulation at both locations, with the largest increase
26
27 34 evident for the turbulent heat fluxes. The synoptic conditions associated with the recent high
28
29 35 melt rates on the proximate Greenland Ice Sheet (GrIS) do not manifest as similarly extreme
30
31 36 melt conditions for our Icelandic location. We also find that the North Atlantic Oscillation
32
33 37 Index is significantly correlated with components of the SEB. This association remains
34
35 38 hidden if the melt rate is assessed in isolation, highlighting the utility of the SEB approach
36
37 39 presented here for assessing synoptic aspects of glacier-climate interactions.
38
39
40
41
42
43
44
45
46
47
48
49
50
51
52
53
54
55
56
57
58
59
60

40

41

42

43

44

Melt energy and synoptic circulation at Vestari Hagafellsjökull

1. Introduction and aims

Melting of the Earth's terrestrially-stored ice is of the utmost hydrological and societal importance. Glaciers and ice caps play a critical role in modulating the seasonal hydrology of mountainous catchments (Jansson et al., 2003; Bradley et al., 2006) and their melting has contributed substantially to recent sea-level rise (Meir et al., 2007; Jacob et al., 2012). Hence, there is a need to understand and quantify the response of the cryosphere to the effects of climate change.

Critical to the rate at which glaciers and ice caps lose mass is the SEB. That is, the net balance of energy at the glacier surface: surplus energy drives melting once the surface has been warmed to 0°C. Much research has addressed the measurement and simulation of the SEB in different climatic environments (e.g. Oerlemans, 2000; Klok and Oerlemans, 2002; Hock and Holmgren, 2005; Giesen et al., 2009; Guðmundsson et al., 2009; Six et al., 2009; Sicart et al., 2011). Such investigations are often used to identify the relative importance of different energy fluxes in driving melting (e.g. Giesen et al., 2009; Nicholson et al., 2012), to calibrate empirical glacier melt models (e.g. Braithwaite, 1995; Arendt and Sharp, 1999; Matthews et al. 2014), or to assess the sensitivity of glacier melt to prescribed increases in air temperatures (e.g. de Wildt et al. 2004; Björnsson et al., 2005). SEB studies therefore play a critical role in understanding how the prevailing weather drives surface melting, and ultimately, the response of glaciers to climate change.

To evaluate the SEB, micrometeorological data from the glacier boundary layer are required. This, however, presents a serious logistical challenge on glaciers, as the remote location and harsh climate typical of glacierized terrain makes continuous data acquisition difficult. As a consequence SEB studies are often brief in duration, which is problematic because the representativeness of such short-term investigations may be limited: the sampling interval

Melt energy and synoptic circulation at Vestari Hagafellsjökull

1
2
3 69 may not represent the full range of SEB conditions experienced at the study location. For
4
5 70 instance, interannual changes in the frequency and duration of particular weather types
6
7 71 (Brazel et al., 1992; Hannah et al., 1999; Konya and Matsumoto, 2010), might result in
8
9 72 observations from a short-lived observation campaign being misleading regarding ‘average’
10
11 73 conditions.

12
13
14 74 Brief SEB investigations are particularly limiting for studies which seek to explore the
15
16 75 synoptic dimension to surface energetics. In general, relatively few researchers have
17
18 76 considered this aspect of glacier-climate interactions from an energy-balance perspective
19
20 77 (Hay and Fitzharris, 1988; Brazel et al., 1992; Hannah et al., 1999). Studies at interannual
21
22 78 resolution are particularly sparse, yet such focus is much required, as an understanding of
23
24 79 how large-scale, low-frequency atmospheric processes ultimately drive melting at the glacier-
25
26 80 scale is important to establish the likely future response of glaciers to climate change. The
27
28 81 micrometeorological processes which ultimately drive surface energy transfer vary at too
29
30 82 small a scale to be resolved by spatially-coarse climate models, and coupling the small- and
31
32 83 large-scales provides a means to address this scale mismatch. A reminder of the importance
33
34 84 of synoptic circulation in modulating glacier-surface energetics has been provided by studies
35
36 85 of the GrIS. Recent research in this region (Fettweis et al., 2011, 2012; Hanna et al., 2013,
37
38 86 2014) has emphasised the role of unprecedented high pressure over the western flank of the
39
40 87 GrIS in driving high, and indeed, record-breaking melt rates over the ice sheet.

41
42
43 88 One way of extending SEB investigations to a length which is more appropriate for exploring
44
45 89 synoptic controls on the surface energetics, is to calculate the SEB using meteorological data
46
47 90 recorded at weather stations located off-glacier (e.g. Klok and Oerlemans, 2002). However,
48
49 91 the low spatial density of such climate-monitoring stations (Jarosch et al., 2012) means that
50
51 92 using these records in place of glacier observations is not a practical solution for studying the
52
53
54
55
56
57
58
59
60

Melt energy and synoptic circulation at Vestari Hagafellsjökull

93 SEB of many of the world's glaciers and ice caps. In this regard, though, gridded reanalyses
94 products may provide a solution.

95 Reanalyses data have their origins in weather forecast initialization. Produced for a regular
96 grid of global coverage by combining raw climate observations with the results of a short-
97 term weather forecast to produce the best estimate of the atmospheric state, they can provide
98 a useful means of gaining insight into meteorological variability in data-sparse regions. In a
99 glaciological capacity, reanalysis data have been used previously to force both temperature-
100 index mass balance models (e.g. Radić and Hock, 2006; Zhang et al., 2007) and energy
101 balance mass balance models (e.g. Hock et al., 2007; Rye et al., 2010), but have been used
102 rarely as a means to extend SEB investigations beyond periods of in-situ observations.

103 In the present study we pursue two main aims related to the points raised above: the first is to
104 assess the feasibility of substituting reanalysis data in place of direct in-situ observation for
105 the purpose of SEB simulation; the second is to establish the role of synoptic circulation in
106 modulating interannual change in the simulated surface energetics. In combining these aims,
107 we seek to demonstrate the value of the bias-corrected reanalysis data for extending SEB
108 series.

109 **2. Data and Methods**

110 **2.1 Overview**

111 The general approach taken here is to use in-situ meteorological data recorded at AWSs to
112 adjust reanalysis data to the glacier climate. Melt energy simulated by a SEB model driven
113 with these data is then compared with the results from a SEB model forced with in-situ AWS
114 data. Close agreement between the two series is taken as confirmation that the reanalysis data
115 can be used to hindcast the SEB (aim 1), which is subsequently undertaken for the duration of

Melt energy and synoptic circulation at Vestari Hagafellsjökull

116 the reanalysis series. The resulting SEB record is then analysed, with specific attention paid
117 to the role of atmospheric circulation in modulating surface energetics (aim 2).

118 **2.2 Study Location and meteorological observations**

119 In-situ meteorological data were obtained from Vestari Hagafellsjökull, an outlet glacier of
120 the Langjökull Ice Cap in Iceland (Figure 1). The climate of Iceland is influenced by the
121 proximate GrIS (~400 km away) and by warm and cold ocean currents which meet of its
122 shores (Hanna et al., 2004). The warm Irminger Current encircles the south, west and north of
123 the island, whilst the cold East Iceland current (a branch of the East Greenland Current) flows
124 south-easterly of Iceland's east coast. The polar front is also normally in close proximity,
125 meaning that air mass transitions are frequent and atmospheric dynamics have a profound
126 effect on Iceland's climate (Einarsson, 1984; Wang and Rogers, 2001; Hanna et al., 2004).
127 These characteristics make our study site well-suited to examining the role of synoptic
128 circulation on surface melt processes. Moreover, given the role of circulation anomalies in
129 driving the unprecedented melt rates observed recently on the proximate GrIS, our record
130 presents the opportunity to explore the extent to which a coherent melt response to synoptic
131 forcing occurs in this region of the North Atlantic.

132 On Vestari Hagafellsjökull, we used data from two AWSs. These stations, located at 500 m
133 and 1100 m (hereafter VH 500 and VH 100, respectively: see bottom right of Figure 1), are
134 described in Guðmundsson et al. (2009) and Matthews et al. (2014). Observations from the
135 AWSs were employed from June-August (hereafter JJA) 2001 to 2007 at VH 500 and JJA
136 2001-2009 at VH 1100.

137 **2.3 Reanalysis data**

Melt energy and synoptic circulation at Vestari Hagafellsjökull

1
2
3 138 To extend the SEB series, the ERA-Interim dataset was used, which is the latest reanalysis
4
5 139 product from the European Centre for Medium Range Weather Forecasting, succeeding the
6
7 140 ERA-40, and spanning the period 1979-present (see Dee et al. (2011)). As input to our SEB
8
9 141 model (described below) the incident radiative fluxes (shortwave and longwave), two-metre
10
11 142 air temperature, two-metre vapour pressure, and two-metre wind speed are required;
12
13 143 appropriate variables were therefore extracted from the ERA-Interim archive
14
15 144 ([http://dataportal.ecmwf.int/data/d/interim daily/](http://dataportal.ecmwf.int/data/d/interim%20daily/)) at $0.75^\circ \times 0.75^\circ$ resolution for the four grid
16
17 145 points closest to our study site (see Table 1). The average height of the reanalysis terrain
18
19 146 across these points is 375 m. The extracted variables were then bilinearly interpolated to the
20
21 147 location of the AWSs (cf. Radić and Hock, 2006; Rye et al. 2010). All reanalysis data were
22
23 148 extracted at three-hourly resolution for the JJA period 1979-2012, before being post-
24
25 149 processed to daily means.
26
27
28
29

30 150 Comparison of the interpolated reanalysis variables with the in-situ observations indicates
31
32 151 appreciable bias (Figure. 2). We therefore adjusted the reanalysed meteorological variables to
33
34 152 the glacier using a quantile-mapping approach (Rye et al., 2010; Hashino et al., 2007). This
35
36 153 non-parametric technique for bias correction has been found to be superior to other statistical
37
38 154 transformations in comparative studies (Hashino et al., 2007; Gudmundsson et al., 2012). The
39
40 155 procedure was implemented via a direct one-to-one mapping of rank-ordered pairs for the
41
42 156 period of coincident observation at each AWS. Outside this interval, the reanalysis variables
43
44 157 were corrected by linearly interpolating between pairs. Values beyond the range witnessed
45
46 158 during the overlapping period are corrected by the minimum/maximum correction factors, as
47
48 159 appropriate. Although this practice is common (Boé et al., 2007; Rye et al., 2010; Themeßl et
49
50 160 al., 2012; Gudmundsson et al., 2012), it is questionable if temporal trends mean that these
51
52 161 minimum/maximum corrections need to be applied often. In such instances, it is
53
54 162 recommended to remove these trends prior to implementing quantile mapping (Beyene et al.,
55
56
57
58
59
60

Melt energy and synoptic circulation at Vestari Hagafellsjökull

1
2
3 163 2010; Dobler et al., 2012). However, this is not an issue here because across all variables and
4
5 164 both locations, a maximum of ~0.3% of the reanalysis series (vapour pressure at VH 1100)
6
7 165 were subject to these extreme correction factors.
8
9

10
11 166 Whilst quantile mapping corrects for biases in the reanalysis data, it does not affect the
12
13 167 temporal agreement with the meteorological variables measured on glacier. This was assessed
14
15 168 in the present study by calculating correlation coefficients between the quantile-mapped
16
17 169 reanalysis data and the observed glacier meteorology.
18
19

20 21 170 **2.4 Surface Energy Balance**

22
23
24 171 The suitability of the SEB model specification employed here (Table 2) has been
25
26 172 demonstrated in previous research (Matthews, 2013; Matthews et al., 2014). We ran this
27
28 173 model at hourly resolution using meteorological data recorded at the glacier AWSs to
29
30 174 generate reference SEB series for each location. When the model was forced with the bias-
31
32 175 corrected reanalysis data, we performed two experiments. The first was designed to validate
33
34 176 the SEB series generated with the reanalysis data. For this, the model was run at daily
35
36 177 resolution for the period when the AWSs were operational with the measured albedo and
37
38 178 emitted longwave radiation used to resolve the net radiative balance. This treatment isolates
39
40 179 the effect of different meteorological forcing data (in-situ *versus* reanalysis) on model
41
42 180 performance. We refer to the SEB series generated with in-situ meteorological data as 'REF',
43
44 181 and use 'REANv', to denote the series obtained using the reanalysis data from this
45
46 182 experiment. Validation of REANv was achieved by comparing this series with water
47
48 183 equivalent melt totals derived from the daily mean energy fluxes in the REF series.
49
50 184 Comparisons were made at daily and annual resolution and correlation coefficients were used
51
52 185 to quantify the agreement between series.
53
54
55
56
57
58
59
60

Melt energy and synoptic circulation at Vestari Hagafellsjökull

1
2
3 186 The second experiment was a hindcasting one, in which the energy balance for the entire 34-
4
5 187 year JJA period was calculated. For this, the albedo was held constant as the mean observed
6
7 188 at each AWS during the observational period, and the emitted longwave radiation was
8
9 189 assumed equal to a blackbody at the melting point. In the case of negative energy balances,
10
11 190 all fluxes were set to zero and no melt was assumed. The SEB series resulting from this
12
13 191 experiment is denoted 'REANh' hereafter. By holding the glacier-surface properties constant
14
15 192 this experiment isolates the role of changes in the prevailing weather in driving SEB
16
17 193 variability. The aim of this approach is not to produce the most accurate simulation of the
18
19 194 SEB over the period 1979-2012, but to assess the long-term variability of potential melt
20
21 195 energy, attributable only to changes in the prevailing weather. By conducting our SEB
22
23 196 experiment according to the above conditions, we could isolate this control on surface
24
25 197 energetics.
26
27
28
29

30
31 198 Trends in REANh were calculated using least-squares linear regression following Box (2002)
32
33 199 and Hanna et al. (2004), with the significance of the slope coefficients (trends) determined
34
35 200 via a two-tailed *t*-test. This treatment therefore only considers sampling uncertainty in
36
37 201 evaluating significance; it makes no provision, for uncertainty stemming from the use of
38
39 202 reanalysis data to calculate REANh, or from the structure of the SEB model itself.
40
41
42

203 **2.5 Atmospheric circulation**

43
44
45
46 204 The role of atmospheric circulation in driving interannual variability in potential melt energy
47
48 205 was assessed by examining the height fields of the 900 hPa surface, and by correlating melt,
49
50 206 and the individual SEB components from REANh, with the North Atlantic Oscillation Index
51
52 207 (NAOI: JJA Hurrell Principal-Component based index; data provided by the Climate Analysis
53
54 208 Section, NCAR, Boulder, USA, and downloaded from:
55
56 209 <http://climatedataguide.ucar.edu/guidance/hurrell-north-atlantic-oscillation-nao-index-pc->
57
58
59
60

Melt energy and synoptic circulation at Vestari Hagafellsjökull

1
2
3 210 based) and the Greenland Blocking Index (GBI). Following Hanna et al. (2013), the GBI was
4
5 211 defined as the mean JJA 500 hPa geopotential height over a region extending from 60-80°N
6
7 212 and 20-80°W. For both the 900 and 500 hPa surfaces, JJA height fields were obtained at
8
9 213 twice-daily resolution from the ERA-Interim archive.

11
12 214 Prior to analysing the role of synoptic circulation in modulating surface energy exchange, all
13
14 215 series (REANh, the 900 hPa height field, and the NAOI/GBI indices) were detrended via
15
16 216 linear regression. This was deemed necessary because average northern hemisphere air
17
18 217 temperatures have risen appreciably during the period 1979-2012 (e.g. Jones et al., 2012), and
19
20 218 such warming (which can enhance the temperature-dependent heat fluxes of the SEB and
21
22 219 raise atmospheric pressure surfaces) may result in spurious associations between the SEB and
23
24 220 atmospheric circulation patterns if not accounted for.

25
26 221 The 900 hPa surface was used because this provides information of atmospheric flow at a
27
28 222 level close to the AWSs (mean atmospheric pressure during the observational period was 950
29
30 223 hPa and 883 hPa at VH 500 and VH 1100, respectively). The relationship between the 900
31
32 224 hPa flow field and REANh was determined by plotting anomaly maps for the five years with
33
34 225 the highest melt rates. These years were identified by ranking melt z -scores averaged between
35
36 226 elevations, so that equal weight was given to both locations when defining high melt years.
37
38 227 We also correlated the 900 hPa height field with REANh to determine linear dependencies of
39
40 228 the SEB on the synoptic flow.

41
42 229 The GBI and the NAOI were used to explore the relation between surface energetics and
43
44 230 synoptic climatology because these indices have been identified as useful indicators of both
45
46 231 GrIS melting (Hanna et al., 2013) and interannual climatological variability in Iceland
47
48 232 (Hanna et al., 2004). All correlations between components of REANh and synoptic climate
49
50
51
52
53
54
55
56
57
58
59
60

Melt energy and synoptic circulation at Vestari Hagafellsjökull

233 indices/flow field were performed at annual (JJA) resolution. Unless otherwise stated, all
234 correlations cited in the text are termed ‘significant’ if they have a p -value less than 0.05.

235 **3. Results**

236 **3.1 Reanalysis climatology**

237 Correlation coefficients quantifying the linear agreement between reanalysis and AWS
238 variables are provided in Table 3. Generally, correlations are strong for all locations, and all
239 are highly significant. Wind speed at VH 500 registers the lowest agreement. However,
240 empirical associations between glacier wind speeds and other near-surface meteorological
241 variables have been noted in Icelandic studies (Björnsson et al., 2005), so we attempted to
242 improve the correspondence between the bias-corrected reanalysis and observed wind speeds
243 by regressing wind speed residuals on other reanalysis variables (see Table 4). The resulting
244 regression model improved the agreement between the corrected reanalysis wind speed and
245 that measured at VH 500 (new $r = 0.61$)

246 **3.2 Surface Energy Balance Modelling**

247 Simulating the SEB using the corrected reanalysis data to drive the melt model resulted in
248 good agreement between the observed and simulated heat fluxes at both daily and annual
249 resolution (Table 5 and Figure 3). The least agreement between series is observed for the
250 latent heat flux at VH 500 when assessed at annual resolution. However, given its relatively
251 minor role in the SEB (Table 5), this does not propagate substantially to the skill in capturing
252 total melt at either elevation. Table 5 also indicates that the bias-correction routine ensures
253 that the relative importance of each of the energy fluxes within the SEB is reproduced
254 closely.

Melt energy and synoptic circulation at Vestari Hagafellsjökull

1
2
3 255 Having established the agreement between SEB simulations forced with the in-situ
4
5 256 observations and the corrected reanalysis data, the SEB was calculated for the entire 34-year
6
7 257 period. The glacier-surface properties (surface roughness, albedo, the outgoing longwave
8
9 258 flux) were held constant for this experiment: changes in simulated melt energy during the
10
11 259 hindcasting period are therefore entirely the result of variability in the prevailing weather.

12
13
14 260 Examination of the resulting SEB series and their trends (Figure 4 and Table 6) indicates that
15
16 261 potential melt energy has increased significantly throughout the period 1979-2012. At both
17
18 262 locations, the sensible, latent and shortwave heat fluxes have contributed positively to the
19
20 263 increase in total melt energy, whilst the longwave heat flux has remained essentially
21
22 264 unchanged. The relative importance of the different energy fluxes within the SEB also shows
23
24 265 appreciable interannual variability (Figure 5), which is, in some cases, systematic. For
25
26 266 example, the percentage of potential melt energy provided by the turbulent heat fluxes has
27
28 267 increased over the hindcasting interval (Figure 6) at a rate which is significant. Thus, the
29
30 268 turbulent heat fluxes have become relatively more important within the SEB during this
31
32 269 period. This would have important implications for empirical glacier melt models calibrated
33
34 270 on our melt series (see Section 4.1).

3.3 Atmospheric Circulation

35
36
37
38
39
40 271
41
42 272 Differenced maps of the 900 hPa geopotential height field for those years with the highest
43
44 273 melt deviations are shown in Figure 7, along with the response of the individual SEB
45
46 274 components. Four of the high-melt years are characterised by a more southerly flow over
47
48 275 western Iceland (1991, 1984, 2003 and 1990), which generally results in an amplification of
49
50 276 the temperature-dependent heat fluxes (sensible, latent and longwave energy components).
51
52 277 The southerly flow responsible for this enhancement results from different configurations of
53
54 278 anomalies in the geopotential height field. In 1984 more southerly flow is a consequence of
55
56
57
58
59
60

Melt energy and synoptic circulation at Vestari Hagafellsjökull

279 higher pressure to the south of Iceland, whilst in 1991, 2003 and 1990, low-pressure
280 anomalies to the south/southeast are responsible.

281 The shortwave heat flux is the main source of melt energy at Vestari Hagafellsjökull, so
282 deviations in this flux have a larger weighting in the overall melt anomaly. This explains why
283 1987 was characterised by high melt rates, despite the fact that only this flux was markedly
284 enhanced. The pressure field during this year was characterised by a high over the GrIS not
285 unlike that which has been associated with enhanced melting of the ice sheet (Fettweiss et al.,
286 2013). Indeed, 1987 was indeed a warm summer for the south west of the ice sheet (see tables
287 3 and 4 in Hanna et al. (2014)). Examination of the correlation maps (Figure 8) demonstrates
288 that the net shortwave flux is generally amplified when pressure is higher over the GrIS and
289 lower over North West Europe. These maps also illustrate that, with the exception of the
290 sensible heat flux, the temperature-dependent SEB components are more pronounced when
291 this pressure pattern is reversed.

292 The detrended melt series are not correlated significantly with the NAOI or GBI at either
293 location (Table 7). For the NAOI this results from the counteracting effects of this index on
294 the temperature-dependent and independent energy fluxes, as the turbulent and longwave
295 SEB components yield correlations with the NAOI which are opposite in sign from that
296 exhibited by net shortwave radiation. The GBI is strongly co-linear with the NAOI ($r = -$
297 0.86); hence, whilst opposite in sign, the association between the GBI and the SEB
298 components is similar to that exhibited by the NAOI, although generally weaker.

4. Discussion

4.1. Reanalysis climatology and surface energy balance modelling

301 Comparisons between the reanalysis data and in-situ meteorological measurements indicated
302 appreciable bias, which is consistent with glacier studies elsewhere (e.g. Rye et al., 2010).

Melt energy and synoptic circulation at Vestari Hagafellsjökull

1
2
3 303 This is not surprising considering the elevation mismatch between the reanalysis model and
4
5 304 our locations (Section 2.3). However, it is unlikely that the bias can be explained only though
6
7 305 this elevational discrepancy. For example, the difference in mean air temperatures recorded at
8
9
10 306 VH 500 and the reanalysis data prior to the bias correction is 3.27°C, corresponding to a
11
12 307 super-adiabatic mean lapse rate of $-2.62^{\circ}\text{C } 100 \text{ m}^{-1}$. Such large biases can instead probably be
13
14 308 explained by the glacier's modifying effect on the overlying atmosphere. In being limited to
15
16 309 the melting point, glaciers typically have a cooling influence on the air above during melt
17
18 310 conditions, simultaneously drying the boundary layer (via condensation) and effecting
19
20 311 katabatic winds (Oerlemans, 2010). These processes are essentially microclimatological
21
22 312 phenomena unresolved by the reanalysis model. This likely explains the relatively modest
23
24 313 association between in-situ and reanalysis wind speeds observed at VH 500, as this location,
25
26 314 in being located further along the flowline, is more frequently exposed to katabatic winds
27
28 315 (Matthews, 2013), whose variability is partially decoupled from the synoptic wind field
29
30 316 (Oerlemans and Grisogono, 2002). The regression model employed in Section 3.1 supports
31
32 317 this interpretation. The coefficients indicate that wind speeds at VH 500 increase as ambient
33
34 318 air temperature and insolation rise (Table 4). Physically, this is consistent with katabatic
35
36 319 forcing because increases in these variables would be expected to amplify the along-glacier
37
38 320 pressure gradient, as warmer ambient air temperatures, augmented by solar heating of the
39
40 321 glacier environs, create a larger near-surface density gradient (cf. Bjornson et al., 2005).

41
42
43
44
45
46 322 Generally, the empirical corrections applied to the reanalysis data were sufficient to result in
47
48 323 good agreement between REF and REANv, which promotes confidence in interpreting
49
50 324 changes in potential melt energy given by REANh. This series indicated amplification of
51
52 325 nearly all components during the period of simulation with only the longwave flux observed
53
54 326 to have remained essentially unchanged, whilst the upward trend in shortwave radiation at
55
56 327 VH 500 was of weak significance. The amplification of the turbulent heat fluxes was
57
58
59
60

Melt energy and synoptic circulation at Vestari Hagafellsjökull

1
2
3 328 particularly compelling, with increases of 28.8 and 61.3% for the sensible and latent heat
4
5 329 fluxes, respectively, for VH 500, and increases of 76.9 and 180.9% at VH 1100. This rise can
6
7 330 be explained by the trend in air temperatures, which have risen at 0.30 and 0.32°C decade⁻¹ at
8
9 331 VH 500 and VH 100, respectively, comparable to documented trends in global-scale land
10
11 332 surface air temperatures observed during this period (0.25 ± 0.05 °C decade⁻¹ to 0.27 ± 0.05
12
13 333 °C decade⁻¹: Jones et al., 2012 and Lawrimore et al., 2011, respectively). The rise in vapour
14
15 334 pressure is approximately consistent with what can be expected from theoretical
16
17 335 considerations of the effects of warmer air temperatures on the atmosphere's saturation
18
19 336 pressure (the Clausius Clapeyron relation: ~7% °C⁻¹), as rates of 6.78 and 5.28% °C⁻¹ were
20
21 337 observed at VH 500 and VH 1100, respectively.
22
23
24
25

26 338 Although exhibiting an upward trend, the shortwave heat fluxes became less important within
27
28 339 the SEB in REAh because their increase did not keep pace with the turbulent heat fluxes.
29
30 340 This would have implications for empirical melt models calibrated on our REAh, which are
31
32 341 sensitive to the relative melt contributions from different energy fluxes. For example, if the
33
34 342 'degree-day factor' (see e.g. Hock, 2003) is calculated at annual resolution on our series, a
35
36 343 significant decrease is observed at VH 1100 (-0.16 mm w.e. d⁻¹ °C⁻¹ a⁻¹). This trend is
37
38 344 consistent with the literature on degree-day factor controls, and their relation to SEB
39
40 345 partitioning (Hock, 2003). Whilst a thorough examination of this point is beyond the scope of
41
42 346 this paper, it is emphasised that such non-stationarity of SEB components should perhaps be
43
44 347 expected at our location, and indeed others, as the climate warms further and the temperature-
45
46 348 dependent heat fluxes are enhanced preferentially.
47
48
49
50

51 349 **4.2 Atmospheric circulation**

52
53
54 350 Addressing the synoptic dimension to this research, we found that years with the highest melt
55
56 351 anomalies were generally characterised by positive deviations of the temperature-dependent
57
58
59
60

Melt energy and synoptic circulation at Vestari Hagafellsjökull

1
2
3 352 heat fluxes resulting from a more southerly flow regime. The recent years characterised by
4
5 353 exceptional melting on the GrIS (primarily since 2007) did not register as similarly extreme
6
7 354 on Vestari Hagafellsjökull. This can be explained by the fact that the recent high-melt events
8
9 355 on the GrIS were a consequence of more persistent anticyclones over the ice sheet (Fettweiss
10
11 356 et al., 2013), and such circulation results in northerly flow over Iceland and the advection of a
12
13 357 relatively cold air mass (Figure 1). In this regard our study is somewhat consistent with
14
15 358 reports of subdued air temperatures and melt rates in Svalbard during the recent period of
16
17 359 extreme melting on the GrIS (Moholdt et al., 2010; Kvamstø et al., 2012). Our results
18
19 360 therefore add to the consensus that, when atmospheric ridging over Greenland is pronounced,
20
21 361 the vigorous melting observed over the GrIS does not extend east of the ice sheet in this
22
23 362 region of the North Atlantic.
24
25
26
27

28 363 Greater insight into synoptic controls on the SEB was granted through correlation analysis
29
30 364 and the clearest associations with the 900 hPa flow field were observed for the radiative and
31
32 365 latent heat fluxes. The shortwave energy flux indicated a tendency to be enhanced when the
33
34 366 pressure field drives north-easterly flow, in a configuration opposite to that favoured by the
35
36 367 longwave and latent heat fluxes. These correlation fields show a high degree of similarity to
37
38 368 the dipole structure of the summertime NAO, which has positive and negative centres over
39
40 369 northwest Europe and Greenland, respectively (Folland et al., 2009), hinting at the
41
42 370 importance of the NAO in modulating surface energetics which was confirmed by inspection
43
44 371 of the NAOI time series.
45
46
47

48
49 372 When the summertime NAO is in a positive phase, circulation is more anticyclonic over the
50
51 373 northwest Europe and more cyclonic over Iceland/southeast Greenland. This results in
52
53 374 southerly flow over a warm ocean surface, advecting a humid air mass over Vestari
54
55 375 Hagafellsjökull and explaining the positive correlation between the NAOI and the latent and
56
57 376 longwave heat fluxes (which depend on the atmospheric vapour pressure). The storm tracks
58
59
60

Melt energy and synoptic circulation at Vestari Hagafellsjökull

1
2
3 377 also pass close to Iceland during this phase of the NAO (Folland et al., 2009), which would
4
5 378 enhance cloud cover over our study site and explains further the correspondence with the
6
7 379 longwave heat flux (which also depends on cloud cover: Sedlar and Hock (2009)). During the
8
9
10 380 negative phase of the summertime NAO, these conditions are reversed: circulation is more
11
12 381 anticyclonic over Iceland and the storm tracks pass to the south, explaining the enhanced
13
14 382 insolation for Vestari Hagafellsjökull inferred from our study.
15
16

17 383 It is a consequence of the opposing sign of the correlations with the NAOI for the
18
19 384 temperature dependent and independent SEB components, that melt itself is not correlated
20
21 385 significantly with this index. This cancelling effect is also evident in Figure 8, where only the
22
23 386 sensible heat flux correlation is 'carried through' to the melt correlation map, as it hasn't been
24
25 387 cancelled by a spatially-coincident correlation of opposite sign. We also observed that the
26
27 388 NAOI is almost universally better correlated with the SEB components than the GBI. This
28
29 389 may be because the NAOI expresses the strength of the dipole pattern, which probably carries
30
31 390 more information about resulting circulation over this region of the North Atlantic (and air
32
33 391 mass advection over Vestari Hagafellsjökull) than the GBI, which emphasises the northern
34
35 392 centre of the dipole (Fang, 2004).
36
37
38
39

40 393 **5. Conclusions**

41
42 394 The main aims of this study were to assess the feasibility of simulating potential glacier
43
44 395 surface melt energy with bias corrected reanalysis data, and to evaluate the role of synoptic
45
46 396 circulation in modulating the surface energetics. Our conclusions from this work can be
47
48 397 summarised:
49
50

51 398 1) Using only simple empirical corrections, the ERA-Interim data captured an
52
53 399 encouraging amount of variance in the observed SEB. Accordingly, we conclude that
54
55
56
57
58
59
60

Melt energy and synoptic circulation at Vestari Hagafellsjökull

1
2
3 400 this technique holds promise for hindcasting series of glacier-surface meteorology and
4
5 401 potential melt energy.
6

7 402 2) Potential melt energy has increased significantly over the period 1979-2012, primarily
8
9 403 as a result of a rise in air temperature. Because the different energy fluxes have not
10
11 404 increased at a uniform rate the relative partitioning of melt energy has also changed,
12
13 405 with the turbulent heat fluxes becoming significantly more important.
14
15

16 406 3) Generally, southerly air flow was observed to drive the highest melt rates on Vestari
17
18 407 Hagafellsjökull through amplification of the temperature-dependent heat fluxes. As
19
20 408 the recent atmospheric ridging over Greenland (which has been associated with the
21
22 409 remarkable melting of the ice sheet) induces a northerly flow over Iceland, similarly
23
24 410 anomalous melt rates have not been experienced for our Icelandic glacier during these
25
26 411 recent years.
27
28

29 412 4) The NAO is an important control on the SEB, particularly the radiative heat fluxes.
30
31 413 Positive correlations were observed for the NAOI with the temperature-dependent
32
33 414 heat fluxes, whilst the net shortwave heat flux exhibited a negative correlation.
34
35 415 Because these correlations are opposite in sign they cancel each other out, resulting in
36
37 416 no significant association between melt itself and the NAOI. The role of the NAO in
38
39 417 modulating surface energetics would therefore not have emerged in our study if the
40
41 418 integrated melt response to synoptic forcing had been assessed in isolation.
42
43
44

45
46 419 We conclude that the approach adopted here provides an important means of understanding
47
48 420 the coupling between local-scale glacier melt processes and synoptic-scale climate
49
50 421 variability, which is required in understanding the response of glaciers to climate change.
51
52

53 422 **References**
54
55
56
57
58
59
60

Melt energy and synoptic circulation at Vestari Hagafellsjökull

- 1
2
3 423 Arendt A and Sharp MJ. 1999. Energy balance measurements on a Canadian high arctic
4
5 424 glacier and their implications for mass balance modeling. *IAHS Publication* **256**: 165-172
6
7
8
9 425 Beyene T, Lettenmaier D and Kabat P. 2010. Hydrologic impacts of climate change on the
10
11 426 Nile River Basin: implications of the 2007 IPCC scenarios. *Climatic Change* **100**: 433–461.
12
13 427 DOI: 10.1007/s10584-009-9693-0
14
15
16 428 Björnsson H, Guðmundsson S, and Pálsson F. 2005. Glacier winds on Vatnajökull ice cap,
17
18 429 Iceland, and their relation to temperatures of its lowland environs. *Annals of Glaciology* **42**:
19
20 430 291-296
21
22
23
24 431 Boé J, Terray L, Habets F and Martin E. 2007. Statistical and dynamical downscaling of the
25
26 432 Seine basin climate for hydro-meteorological studies. *International Journal of Climatology*
27
28 433 **27**: 1643–1655. DOI:10.1002/joc.1602
29
30
31
32 434 Box JE. 2002. Survey of Greenland instrumental temperature records: 1873–
33
34 435 2001. *International Journal of Climatology* **22**: 1829-1847. DOI: 10.1002/joc.852
35
36
37 436 Bradley RS, Vuille M, Diaz HF and Vergara W. 2006. Threats to water supplies in the
38
39 437 tropical Andes. *Science* **312**: 1755-1756. DOI: 10.1126/science.1128087
40
41
42
43 438 Braithwaite RJ. 1995. Positive degree-day factors for ablation on the Greenland ice sheet
44
45 439 studied by energy balance modeling. *Journal of Glaciology* **41**: 153-160
46
47
48
49 440 Brazel AJ, Chambers FB and Kalkstein LS. 1992. Summer energy balance on West Gulkana
50
51 441 Glacier, Alaska, and linkages to a temporal synoptic index. *Zeitschrift für Geomorphologie*
52
53 442 **86**: 15-34
54
55
56
57
58
59
60

Melt energy and synoptic circulation at Vestari Hagafellsjökull

- 1
2
3 443 de Wildt MDR, Oerlemans J and Björnsson H. 2004. A calibrated mass balance model for
4
5 444 Vatnajökull. *Jökull* **52**: 1-20
6
7
8
9 445 Dee DP, Uppala SM, Simmons AJ, Berrisford P, Poli P, Kobayashi S, Andrae U, Balmaseda
10
11 446 MA, Balsamo G, Bauer P, Bechtold P, Beljaars ACM, Van de Berg L, Bidlot J, Bormann N,
12
13 447 Delsol C, Dragani R, Fuentes M, Geer AJ, Haimberger L, Healy SB, Hersbach H, Hólm EV,
14
15 448 Isaksen L, Kållberg P, Köhler M, Matricardi M, McNally AP, Monge-sanz BM, Morcrette J,
16
17 449 Park B, Peubey C, de Rosnay P, Tavolato C, Thépaut J and Vitart F. 2011. The ERA-Interim
18
19 450 reanalysis: configuration and performance of the data assimilation system. *Quarterly Journal*
20
21 451 *of the Royal Meteorological Society* **137**: 553-597. DOI: 10.1002/qj.828
22
23
24
25 452 Dobler C, Hagemann S, Wilby RL and Stötter J. 2012. Quantifying different sources of
26
27 453 uncertainty in hydrological projections in an Alpine watershed. *Hydrology & Earth System*
28
29 454 *Sciences* **16**: 4343–4360. DOI: 10.5194/hess-16-4343-2012
30
31
32
33 455 Einarsson MÁ. 1984. *Climate of Iceland*. In: Van Loon H. ed. *Climates of the Oceans*. First
34
35 456 edn. Amsterdam: 673-697
36
37
38
39 457 Fang ZF. 2004. Statistical relationship between the northern hemisphere sea ice and
40
41 458 atmospheric circulation during wintertime. In *Observation, Theory and Modeling of*
42
43 459 *Atmospheric Variability. World Scientific Series on Meteorology of East Asia*, Zhu X (ed).
44
45 460 World Scientific Publishing Company: Singapore; 131–141
46
47
48
49 461 Fettweis X, Mabilille G, Erpicum M, Nicolay S and Broeke M. 2011. The 1958-2009
50
51 462 Greenland ice sheet surface melt and the mid-tropospheric atmospheric circulation. *Climate*
52
53 463 *Dynamics* **36**: 139-159. DOI: 10.1007/s00382-010-0772-8
54
55
56
57
58
59
60

Melt energy and synoptic circulation at Vestari Hagafellsjökull

- 1
2
3 464 Fettweis X, Hanna E, Lang C, Belleflamme A, Erpicum M and Gallée H. 2013. Brief
4
5 465 communication: Important role of the mid-tropospheric atmospheric circulation in the recent
6
7 466 surface melt increase over the Greenland ice sheet. *The Cryosphere* **7**: 241-248. DOI:
8
9 467 10.5194/tc-7-241-2013
10
11
12
13 468 Folland CK, Knight J, Linderholm HW, Fereday D, Ineson S and Hurrell JW. 2009. The
14
15 469 summer North Atlantic Oscillation: past, present, and future. *Journal of Climate* **22**: 1082-
16
17 470 1103. DOI: 10.1175/2008JCLI2459.1
18
19
20
21 471 Giesen RH, Andreassen LM, Broeke MR and Oerlemans J. 2009. Comparison of the
22
23 472 meteorology and surface energy balance at Storbreen and Midtdalsbreen, two glaciers in
24
25 473 southern Norway. *The Cryosphere* **3**: 57-74. DOI: 10.5194/tc-3-57-2009
26
27
28
29 474 Gudmundsson L, Bremnes JB, Haugen JE and Engen-Skaugen T. 2012. Technical Note:
30
31 475 Downscaling RCM precipitation to the station scale using statistical transformations--a
32
33 476 comparison of methods. *Hydrology & Earth System Sciences* **16**: 3383-3390. DOI:
34
35 477 10.5194/hess-16-3383-2012
36
37
38
39 478 Guðmundsson S, Björnsson H, Pálsson F and Haraldsson HH. 2009. Comparison of energy
40
41 479 balance and degree-day models of summer ablation on the Langjökull ice cap, SW-Iceland.
42
43 480 *Jökull* **59**: 1-17
44
45
46
47 481 Hanna E, Fettweis X, Mernild SH, Cappelen J, Ribergaard MH, Shuman CA and Mote TL.
48
49 482 2014. Atmospheric and oceanic climate forcing of the exceptional Greenland ice sheet
50
51 483 surface melt in summer 2012. *International Journal of Climatology* **34**: 1022-1037. DOI:
52
53 484 10.1002/joc.3743
54
55
56
57
58
59
60

Melt energy and synoptic circulation at Vestari Hagafellsjökull

- 1
2
3 485 Hanna E, Jónsson T and Box JE. 2004. An analysis of Icelandic climate since the nineteenth
4
5 486 century. *International Journal of Climatology* **24**: 1193-1210. DOI: 10.1002/joc.1051
6
7
8
9 487 Hanna E, Jones JM, Cappelen J, Mernild SH, Wood L, Steffen K, Huybrechts, P. 2013. The
10
11 488 influence of North Atlantic atmospheric and oceanic forcing effects on 1900-2010 Greenland
12
13 489 summer climate and ice melt/runoff. *International Journal of Climatology* **33**: 862-880. DOI:
14
15 490 10.1002/joc.3475
16
17
18
19 491 Hannah DM, Gurnell AM and McGregor GR. 1999. Identifying links between large-scale
20
21 492 atmospheric circulation and local glacier ablation climates in the French Pyrenees. *IAHS*
22
23 493 *Publication* **256**: 155-164
24
25
26 494 Hashino T, Bradley AA and Schwartz SS. 2007. Evaluation of bias-correction methods for
27
28 495 ensemble streamflow volume forecasts. *Hydrology & Earth System Sciences* **11**: 939-950.
29
30 496 DOI: 10.5194/hess-11-939-2007
31
32
33
34 497 Hay JE and Fitzharris BB. 1988. A comparison of the energy balance and bulk - aerodynamic
35
36 498 approaches for estimating glacier melt. *Journal of Glaciology* **34**: 144-153
37
38
39
40 499 Hock R. 2003. Temperature index melt modelling in mountain areas. *Journal of Hydrology*
41
42 500 **282**: 104-115. DOI: 10.1016/s0022-1694(03)00257-9
43
44
45
46 501 Hock R, Radic V and de Woul M. 2007. Climate sensitivity of Storglaciären, Sweden: an
47
48 502 intercomparison of mass-balance models using ERA-40 re-analysis and regional climate
49
50 503 model data. *Annals of glaciology* **46**: 342-348. DOI: 10.3189/172756407782871503
51
52
53
54 504 Hock R and Holmgren B. 2005. A distributed surface energy balance model for complex
55
56 505 topography and its application to Storglaciären, Sweden. *Journal of Glaciology* **51**: 25-36.
57
58 506 DOI: 10.3189/172756505781829566
59
60

Melt energy and synoptic circulation at Vestari Hagafellsjökull

- 1
2
3 507 Jacob T, Wahr J, Pfeffer WT and Swenson S. 2012. Recent contributions of glaciers and ice
4
5 508 caps to sea level rise. *Nature* **482**: 514-518. DOI: 10.1038/nature10847
6
7
8
9 509 Jones PD, Lister DH, Osborn TJ, Harpham C, Salmon M, and Morice CP. 2012. Hemispheric
10
11 510 and large-scale land-surface air temperature variations: An extensive revision and an update
12
13 511 to 2010. *Journal of Geophysical Research: Atmospheres* **117**.
14
15
16 512 Jansson P, Hock R and Schneider T. 2003. The concept of glacier storage: a review. *Journal*
17
18 513 *of Hydrology* **282**: 116-129. DOI: 10.1016/S0022-1694(03)00258-0
19
20
21
22 514 Jarosch AH, Anslow FS and Clarke GK. 2012. High-resolution precipitation and temperature
23
24 515 downscaling for glacier models. *Climate Dynamics*, **38**: 391-409. DOI: 10.1007/s00382-010-
25
26 516 0949-1
27
28
29
30 517 Klok EJ and Oerlemans J. 2002. Model study of the spatial distribution of the energy and
31
32 518 mass balance of Morteratschgletscher, Switzerland. *Journal of Glaciology* **48**: 505-518. DOI:
33
34 519 10.3189/172756502781831133
35
36
37
38 520 Konya K and Matsumoto T. 2010. Influence of weather conditions and spatial variability on
39
40 521 glacier surface melt in Chilean Patagonia. *Theoretical Applied Climatology* **102**: 139-149.
41
42 522 DOI: 10.1007/s00704-009-0248-0
43
44
45 523 Kvamstø NG, Steinskog DJ, Stephenson DB, and Tjøstheim DB. 2012. Estimation of trends
46
47 524 in extreme melt-season duration at Svalbard. *International Journal of Climatology*, **32**: 2227-
48
49 525 2239. DOI: 10.1002/joc.3395
50
51
52
53 526 Lawrimore JH, Menne MJ, Gleason BE, Williams CN, Wuertz DB, Vose RS, and Rennie J.
54
55 527 2011. An overview of the Global Historical Climatology Network monthly mean temperature
56
57 528 data set, version 3. *Journal of Geophysical Research* **116**. DOI: 10.1029/2011JD016187
58
59
60

Melt energy and synoptic circulation at Vestari Hagafellsjökull

- 1
2
3 529 Matthews TKR. 2013. *Glacier-climate interactions: a synoptic approach*. PhD thesis,
4
5 530 Loughborough University. Available at: <https://dspace.lboro.ac.uk/2134/12558>.
6
7
8
9 531 Matthews T, Hodgkins R, Wilby RL, Guðmundsson S, Pálsson F, Björnsson H, and Carr S.
10
11 532 2014. Conditioning temperature-index model parameters on synoptic weather types for
12
13 533 glacier melt simulations. *Hydrological Processes*. DOI: 10.1002/hyp.10217
14
15
16 534 Meier MF, Dyurgerov MB, Rick UK, O'Neel S, Pfeffer WT, Anderson RS, Anderson SP and
17
18 535 Glazovsky AF. 2007. Glaciers dominate eustatic sea-level rise in the 21st century. *Science*
19
20 536 **317**: 1064. DOI: 10.1126/science.1143906
21
22
23
24 537 Moholdt G, Nuth C, Hagen JO, and Köhler, J. 2010. Recent elevation changes of Svalbard
25
26 538 glaciers derived from ICESat laser altimetry. *Remote Sensing of Environment*. **114**: 2756–
27
28 539 2767. DOI:10.1016/j.rse.2010.06.008
29
30
31
32 540 Nicholson L, Prinz R, Mölg T, and Kaser G. 2012. Micrometeorological conditions and
33
34 541 surface mass and energy fluxes on Lewis glacier, Mt Kenya, in relation to other tropical
35
36 542 glaciers. *The Cryosphere* **7**: 5181-5224. DOI: 10.5194/tc-7-1205-2013
37
38
39
40 543 Oerlemans J. 2010. *The microclimate of valley glaciers*. First edn. Utrecht: Igitur, Utrecht
41
42 544 Publishing and Archiving Services, Universiteitsbibliotheek Utrecht
43
44
45 545 Oerlemans J. 2000. Analysis of a 3 year meteorological record from the ablation zone of
46
47 546 Morteratschgletscher, Switzerland: energy and mass balance. *Journal of Glaciology* **46**: 571-
48
49 547 579. DOI: 10.3189/172756500781832657
50
51
52
53 548 Oerlemans J and Grisogono B. 2002. Glacier winds and parameterisation of the related
54
55 549 surface heat fluxes. *Tellus A* **54**: 440-452. DOI: 10.1034/j.1600-0870.2002.201398.x
56
57
58
59
60

Melt energy and synoptic circulation at Vestari Hagafellsjökull

- 1
2
3 550 Radić V and Hock R. 2006. Modelling future glacier mass balance and volume changes using
4
5 551 ERA-40 reanalysis and climate models: A sensitivity study at Storglaciären, Sweden, *Journal*
6
7 552 *of Geophysical Research: Earth Surface* **111**. DOI: 10.1029/2005JF000440
8
9
10
11 553 Rye CJ, Arnold NS, Willis IC. and Kohler J. 2010. Modeling the surface mass balance of a
12
13 554 high Arctic glacier using the ERA-40 reanalysis. *Journal of Geophysical Research: Earth*
14
15 555 *Surface* **115**. DOI: 10.1029/2009JF001364
16
17
18 556 Sedlar J and Hock R. 2009. Testing longwave radiation parameterizations under clear and
19
20 557 overcast skies at Storglaciären, Sweden. *The Cryosphere* **3**: 75-84. DOI: 10.5194/tc-3-75-
21
22 558 2009
23
24
25
26 559 Sicart JE, Hock R, Ribstein P, Litt, M and Ramirez E. 2011. Analysis of seasonal variations
27
28 560 in mass balance and meltwater discharge of the tropical Zongo Glacier by application of a
29
30 561 distributed energy balance model. *Journal of Geophysical Research: Atmospheres* **116**. DOI:
31
32 562 10.1029/2010JD015105
33
34
35
36 563 Six D, Wagnon P, Sicart JE and Vincent C. 2009. Meteorological controls on snow and ice
37
38 564 ablation for two contrasting months on Glacier de Saint-Sorlin, France. *Annals of glaciology*
39
40 565 **50**: 66-72. DOI: 10.3189/172756409787769537
41
42
43
44 566 Themeßl MJ, Gobiet A and Heinrich G. 2012. Empirical-statistical downscaling and error
45
46 567 correction of regional climate models and its impact on the climate change signal. *Climatic*
47
48 568 *Change* **112**: 449–468. DOI:10.1007/s10584-011-0224-4
49
50
51
52 569 Wang CC and Rogers JC. 2001. A Composite Study of Explosive Cyclogenesis in Different
53
54 570 Sectors of the North Atlantic. Part I: Cyclone Structure and Evolution. *Monthly Weather*
55
56 571 *Review* **129**: 1481-1499. DOI: 10.1175/1520-0493(2001)129<1481:ACSOEC>2.0.CO;2
57
58
59
60

Melt energy and synoptic circulation at Vestari Hagafellsjökull

1
2
3 572 Zhang J, Bhatt US, Tangborn WV and Lingle CS. 2007. Climate downscaling for estimating
4
5 573 glacier mass balances in northwestern North America: Validation with a USGS benchmark
6
7 574 glacier. *Geophysical Research Letters* **34**. DOI: 10.1029/2007GL031139
8
9

10
11 **Figure captions:**

12
13
14 576 **Table 7.** Correlations, and their significance, between REANh and the NAOI and GBI. Note that p is the
15
16 577 probability of obtaining a correlation coefficient as large (in an absolute sense) as that given if the null
17
18 578 hypothesis (that $r = 0$) is true
19

20
21 579 **Figure 1.** Location of study sites. Right-hand-side shows the climatological setting of Iceland, in terms of near-
22
23 580 surface air temperatures (top) and sea surface temperatures (bottom). The air temperatures were obtained from
24
25 581 the 1981-2010 NCEP1 climatology (Kalanay et al., 1996) and the sea surface temperatures were calculated by
26
27 582 averaging the long-term monthly mean values over the period 1971-2000 from the NOAA_OI_SST_V2 dataset,
28
29 583 provided by the NOAA/OAR/ESRL PSD (<http://www.esrl.noaa.gov/psd/>). Left-hand-side: the Langjökull ice
30
31 584 cap and its situation within Iceland (inset). The locations of the two AWSs (VH 500 and VH 1100) are also
32
33 585 indicated
34

35 586 **Figure 2.** Empirical cumulative distributions for the observed and reanalysis variables. Note that the reanalysis
36
37 587 variables have been bilinearly interpolated to the location of the AWSs
38

39
40 588 **Figure 3.** Comparisons between the REF and REANv series when compared at daily (top) and annual (bottom)
41
42 589 resolution. Note that correlation coefficients quantifying the linear relationship between these series are
43
44 590 provided in Table 4. Energy fluxes in the legend are abbreviated as follows: SHF: sensible heat flux, LHF: latent
45
46 591 heat flux, SW: net shortwave radiation and LW: net longwave radiation
47

48
49 592 **Figure 4.** The hindcast SEB series. Hindcast fluxes and melt are shown annually (JJA); the totals are derived by
50
51 593 summing all daily JJA contributions to melting for each year. Error bars for each series indicate ± 1 standard
52
53 594 deviation of the residuals for annual totals when compared to REF, deduced from inspecting the series
54
55 595 illustrated in Figure 3. The dotted lines were fit with linear regression: see Table 6 for their slopes and
56
57 596 significance. Energy fluxes are abbreviated as outlined in Figure 3 caption
58
59
60

Melt energy and synoptic circulation at Vestari Hagafellsjökull

1
2
3 597 **Figure 5.** Annual (JJA) contributions of each of the energy fluxes to total melt at both elevations during the
4
5 598 hindcasting period (1979-2012), illustrating the relative contribution to melting from each of the energy fluxes

6
7
8 599 **Figure 6.** The fraction (expressed as a percentage) of total annual melt energy (JJA) provided by the turbulent
9
10 600 heat fluxes (sensible + latent), relative to that contributed by the radiative heat fluxes (shortwave + longwave).
11 601 The dotted lines indicate the least-squares linear fit. The trends are both significant (at $p = 0.05$) according to a
12 602 two-tailed t -test. Uncertainty bars ($\pm\delta$) are calculated: $\delta = \sqrt{\left[\frac{\delta SHF^2 + \delta LHF^2}{(SHF + LHF)^2}\right] + \left[\frac{\delta SW^2 + \delta LW^2}{(SW + LW)^2}\right]}$ K , where K is the
13
14 603 fraction plotted and the errors terms for the individual energy components (δx), are denoted as given in Figure
15
16 604 3 caption, and whose values were estimated as outlined in the caption of Figure 4

17
18 605 **Figure 7.** Anomaly maps for the five years with the highest melt rate (see Section 2.5). Left-hand-side: the 900
19
20 606 hPa height (colormap), and wind vector anomalies (arrows). Because the gridded data are linearly detrended,
21
22 607 the anomaly fields plotted for each JJA period were calculated simply by averaging the grid-point values for the
23
24 608 year in question (as the detrended gridpoint series have means of zero). The 'u' and 'v' wind vectors required
25
26 609 for this plot were obtained from the ERA-Interim archive as monthly means of daily means. Right-hand-side:
27
28 610 contributions to melting from the detrended components of the REANh series for JJA in the years indicated

29
30 611 **Figure 8.** Correlations (ρ), at annual (JJA) resolution, between components of REANh and the 900 hPa height
31
32 612 field. The white line bounds correlations that are significantly different from zero at $p < 0.05$. Note that all
33
34 613 series are detrended with respect to time. Energy flux abbreviations are outlined in Figure 3 caption

35
36
37 614

38
39
40 615

41
42
43 616

44
45
46 617

47
48
49 618

50
51
52 619

53
54
55 620

56
57
58 621

Melt energy and synoptic circulation at Vestari Hagafellsjökull

622 **Table 1.** Meteorological variables required for the SEB model (described in the text and in Table 2), and the
 623 meteorological variables used from the ERA-Interim archive to satisfy these requirements. The column labelled
 624 ‘transformations’ details the relevant treatment applied to the reanalysis variables needed to maintain
 625 compatibility with the required input variable

Required input variable	Reanalysis variable used	Transformation
Two-metre air temperature	Two-metre air temperature	<i>NA</i>
Two-metre vapour pressure (<i>e</i>)	Two-metre dewpoint temperature (T_d)	$e = e_0 \exp\left[-\left(\frac{1}{T_d} - \frac{1}{T_0}\right) L RV^{-1}\right]$ with $e_0 = 610.8$ Pa; $T_0 = 273.15K$; L = the latent heat of vaporization (2.5×10^6 J kg ⁻¹); RV = the gas constant for water vapour (461 J kg ⁻¹). Note that T_d is in Kelvin.
Two-metre wind speed (W_s)	10-metre U-component (U) of wind speed; 10-metre V-component (V) of wind speed	$W_s = \sqrt{U^2 + V^2}$
Incident shortwave radiation	Surface solar radiation downwards	<i>NA</i>
Incident longwave radiation	Surface thermal radiation downwards	<i>NA</i>

626

627

628

629

630

631

632

Melt energy and synoptic circulation at Vestari Hagafellsjökull

633 **Table 2.** Details of energy fluxes' treatment within the SEB model. See text in Section 2.4 for further
 634 explanation

Model for calculating the SEB (Q):			
$Q = Q_H + Q_L + Q_{SW} + Q_{LW} + Q_R + Q_G$			
Quantity	Procedure for calculation	Associated parameters/ parameterisations	Treatment/value of parameters
Turbulent heat (sensible: Q_H and latent: Q_L heat)	Bulk aerodynamic method	Roughness length of momentum	Ice: 10 mm Firn: 2 mm Snow: 0.1 mm
		Roughness lengths of water vapour and temperature	Modelled according to Andreas (1987).
		Stability corrections for turbulent heat flux calculations	Non-linear expressions of Beljaars and Holtslag (1991) used for stable conditions (glacier surface temperature below air temperature); equations of Paulson (1970) and Dyer (1974) applied for unstable case.
		Glacier surface temperature	Assumed to be at the melting point (0°C).
Net shortwave (Q_{SW})	Incident flux minus reflected flux	Reflected shortwave radiation	Taken from measurements during period when the reanalysis-driven SEB is validated; calculated by multiplying the incident flux by the mean observed albedo during the measurement period for the hindcasting experiment (1979-2012). See text for more details.
Net longwave (Q_{LW})	Incident flux minus the flux emitted by the glacier surface	Emitted longwave radiation	Measured values used during validation period; emission assumed equal to a blackbody at the melting point during the hindcasting experiment.
Rain (Q_R) and Ground (Q_G)	<i>Neglected</i>	<i>Neglected</i>	<i>Neglected</i>

635

636

Melt energy and synoptic circulation at Vestari Hagafellsjökull

637 **Table 3.** Correlation coefficients between the daily mean values of the meteorological variables observed at the
638 AWSs, and the bias-corrected (quantile-mapped) ERA-Interim reanalysis variables. Note that all correlations are
639 highly significant ($p < 0.01$)

	VH 500	VH 1100
Air temperature	0.73	0.88
Wind speed	0.50	0.67
Vapour pressure	0.77	0.85
Incident shortwave radiation	0.78	0.79
Incident longwave radiation	0.76	0.67

640

641

642

643

644

645

646

647

648

649

650

651

652

653

654

655

Melt energy and synoptic circulation at Vestari Hagafellsjökull

656 **Table 4.** Details of the regression model used to correct the bias corrected reanalysis wind speed at VH 500.
 657 Note that t is the student's t -statistic, and p indicates the probability of obtaining an absolute value of t larger
 658 than given in the preceding column if the null hypothesis (that $\beta_i = 0$) is true

Regression model summary: Glacier wind speed can be written: $Wspd_{ERA_bc} - y$; where $Wspd_{ERA_bc}$ is the bias-corrected ERA-Interim wind speed and 'y' is $Wspd_{ERA_bc}$ minus the observed glacier wind speed. 'y' can be written: $y = \beta_0 x_0 + \beta_1 x_1 + \beta_2 x_2 + \epsilon$, where x_i are variables, β_i are regression coefficients and ϵ is a random error term. Below, values of the regression coefficients used to estimate 'y' are provided.

Variable: x_i	Coefficient: β_i (units)	t	p
Constant ($x_0 = 1$)	3.9713 ($m\ s^{-1}$)	14.56	0.00
Raw ERA-Interim 2-metre air temperature (x_1)	-0.3490 ($m\ s^{-1}\ ^\circ C^{-1}$)	-11.41	0.00
Bias-corrected ERA-Interim incident shortwave radiation (x_2)	-0.0060 ($m\ s^{-1}\ W^{-1}\ m^2$)	-9.07	0.00
N = 642; Adj. $R^2 = 0.28$			

659

660

661

662

663

664

665

666

667

668

669

670

671

672

673

Melt energy and synoptic circulation at Vestari Hagafellsjökull

674 **Table 5.** Relative contribution (%) to melting of the energy fluxes calculated with SEB when forced with in-situ
 675 AWS observations (REF) and with the bias-corrected ERA-Interim reanalysis data (REANv). Correlation
 676 coefficients between the REANv and REF series are also given, which are nearly all significant at $p < 0.01$; those
 677 correlations that are not significant at the 99% confidence interval for a two-tailed t -test are marked with
 678 asterisks: *is significant at the 95% confidence interval ($p = 0.02$); ** is not significant at the 90% confidence
 679 interval ($p = 0.11$). Note that REANv is calculated using a regression-based correction to the wind speed at VH
 680 500 (see text in Section 3.1 and Table 4)

	VH 500				VH 1100			
	REF (%)	REANv (%)	r (daily)	r (annual)	REF (%)	REANv (%)	r (daily)	r (annual)
Sensible Heat	26.96	27.45	0.78	0.82*	19.81	20.05	0.74	0.84
Latent heat	9.83	10.35	0.81	0.65**	6.03	6.18	0.74	0.84
Shortwave radiation	63.92	62.89	0.79	0.93	92.03	89.16	0.84	0.98
Longwave radiation	-0.71	-0.69	0.75	0.95	-17.88	-15.39	0.55	0.90
Melt	-	-	0.79	0.98	-	-	0.87	0.96

681

682

683

684

685

686

687

688

689

690

691

692

Melt energy and synoptic circulation at Vestari Hagafellsjökull

693 **Table 6.** REANh trends and their significance (p) during the hindcasting period (1979-2012). See the text in
 694 Section 2.4 for further details

	VH 500		1100 m	
	slope (mm w.e. a ⁻²)	p	slope (mm w.e. a ⁻²)	p
Sensible heat flux	11.68	0.00	6.51	0.00
Latent heat flux	7.46	0.01	2.81	0.05
Net shortwave radiation	10.94	0.16	7.79	0.05
Net longwave radiation	1.40	0.63	-0.95	0.72
Melt	31.47	0.00	16.15	0.01

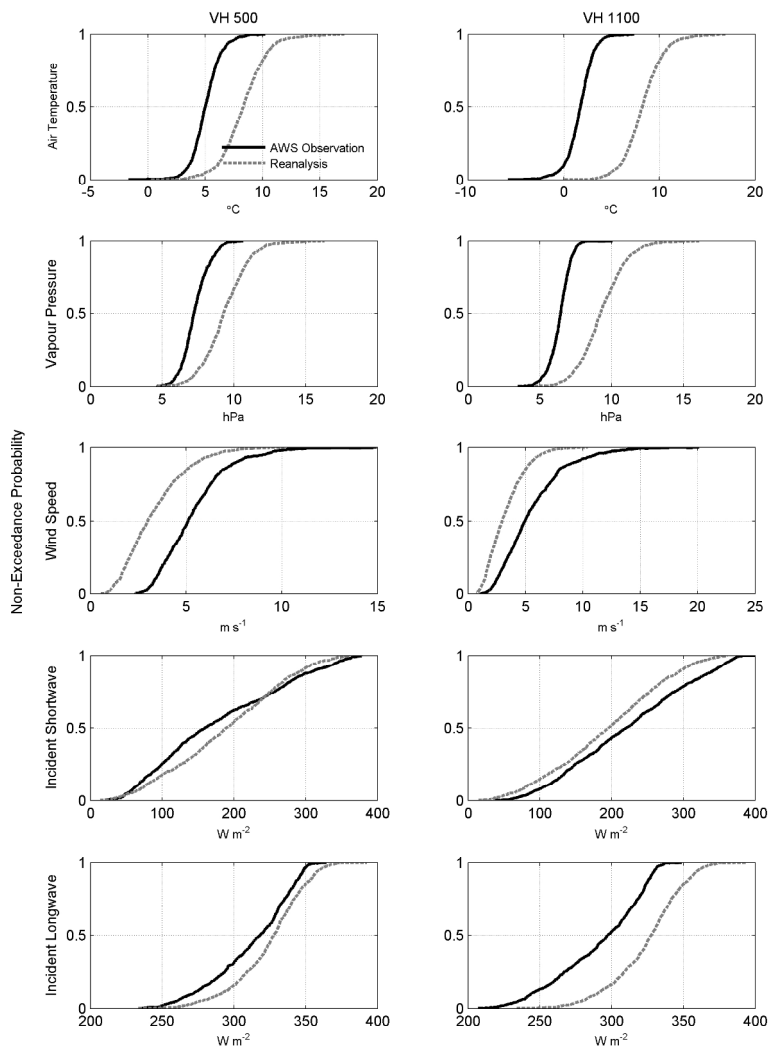
Melt energy and synoptic circulation at Vestari Hagafellsjökull

716 **Table 7.** Correlations, and their significance, between REANh and the NAOI and GBI. Note that p is the
 717 probability of obtaining a correlation coefficient as large (in an absolute sense) as that given if the null
 718 hypothesis (that $r = 0$) is true

SEB Component	NAOI		GBI		
	r	p	r	p	
VH 500	Sensible heat flux	0.12	0.50	0.05	0.78
	Latent heat flux	0.30	0.08	-0.08	0.66
	Net shortwave radiation	-0.66	0.00	0.54	0.00
	Net longwave radiation	0.46	0.01	-0.23	0.20
	Melt	-0.20	0.26	0.33	0.06
VH 1100	Sensible heat flux	0.05	0.78	0.17	0.33
	Latent heat flux	0.40	0.02	-0.15	0.38
	Net shortwave radiation	-0.51	0.00	0.53	0.00
	Net longwave radiation	0.51	0.00	-0.34	0.05
	Melt	0.04	0.80	0.18	0.31

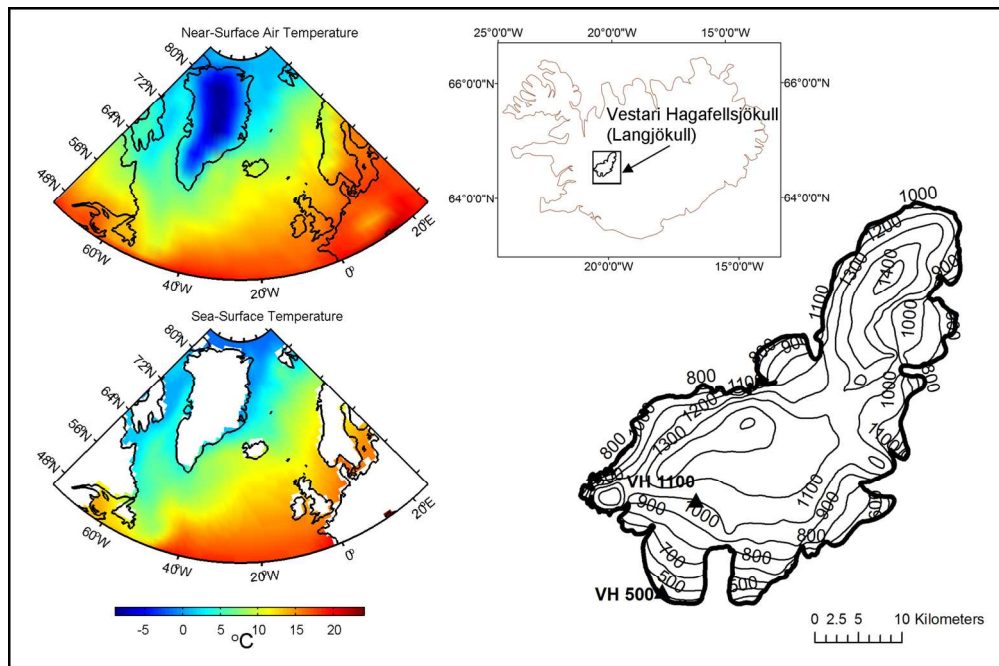
719

1
2
3
4
5
6
7
8
9
10
11
12
13
14
15
16
17
18
19
20
21
22
23
24
25
26
27
28
29
30
31
32
33
34
35
36
37
38
39
40
41
42
43
44
45
46
47
48
49
50
51
52
53
54
55
56
57
58
59
60



205x287mm (300 x 300 DPI)

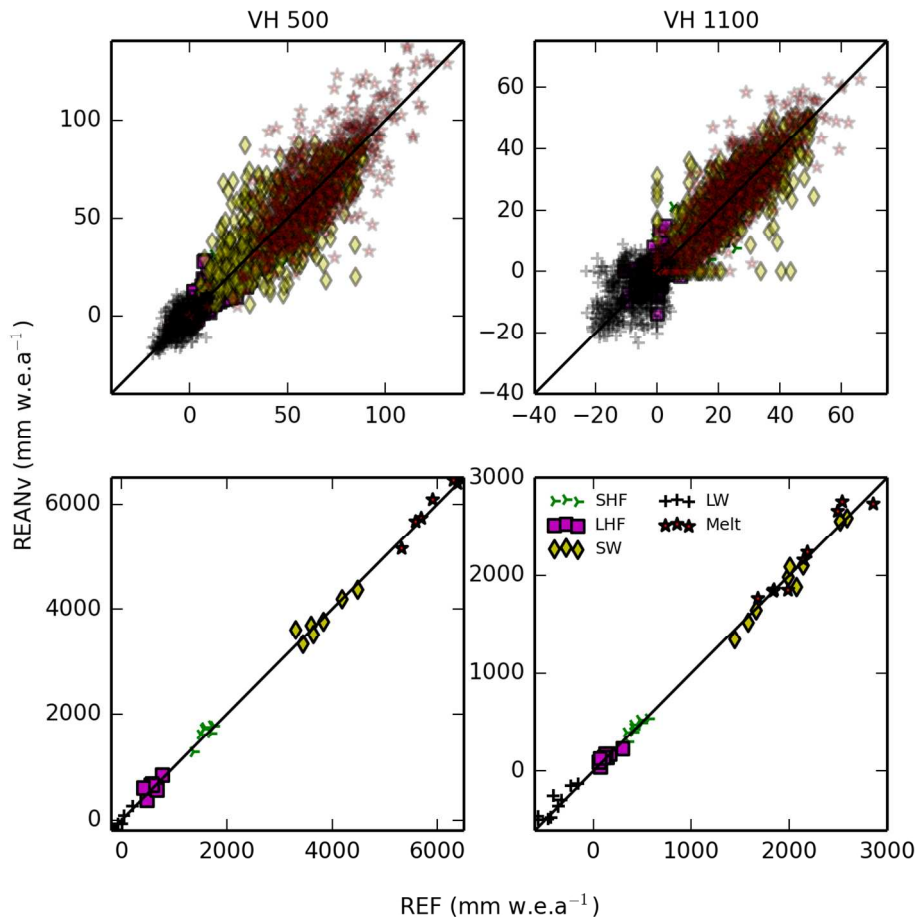
1
2
3
4
5
6
7
8
9
10
11
12
13
14
15
16
17
18
19
20
21
22
23
24
25
26
27
28
29
30
31
32
33
34
35
36
37
38
39
40
41
42
43
44
45
46
47
48
49
50
51
52
53
54
55
56
57
58
59
60



166x110mm (300 x 300 DPI)

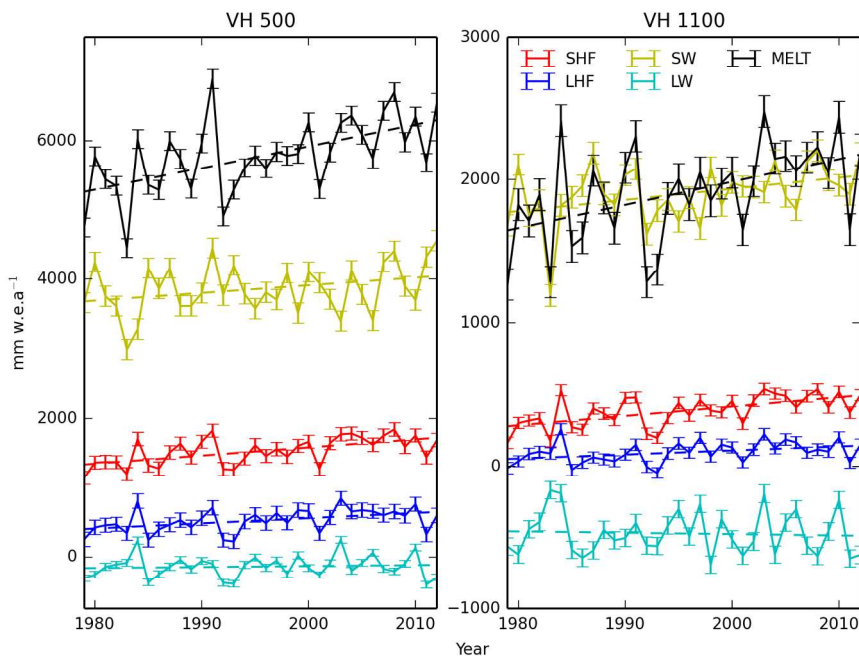
iew Only

1
2
3
4
5
6
7
8
9
10
11
12
13
14
15
16
17
18
19
20
21
22
23
24
25
26
27
28
29
30
31
32
33
34
35
36
37
38
39
40
41
42
43
44
45
46
47
48
49
50
51
52
53
54
55
56
57
58
59
60



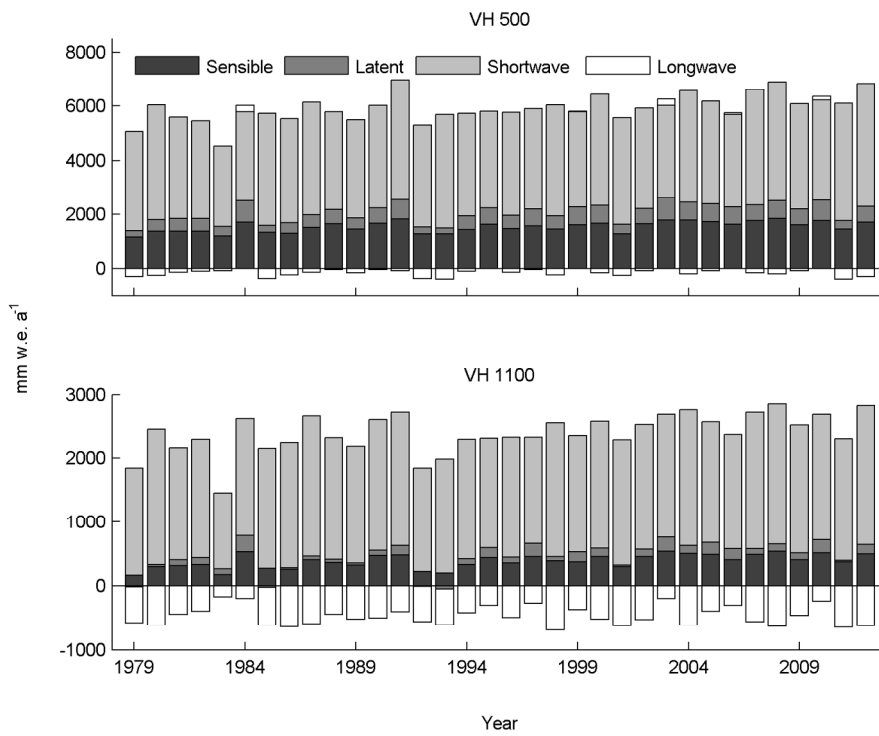
127x127mm (300 x 300 DPI)





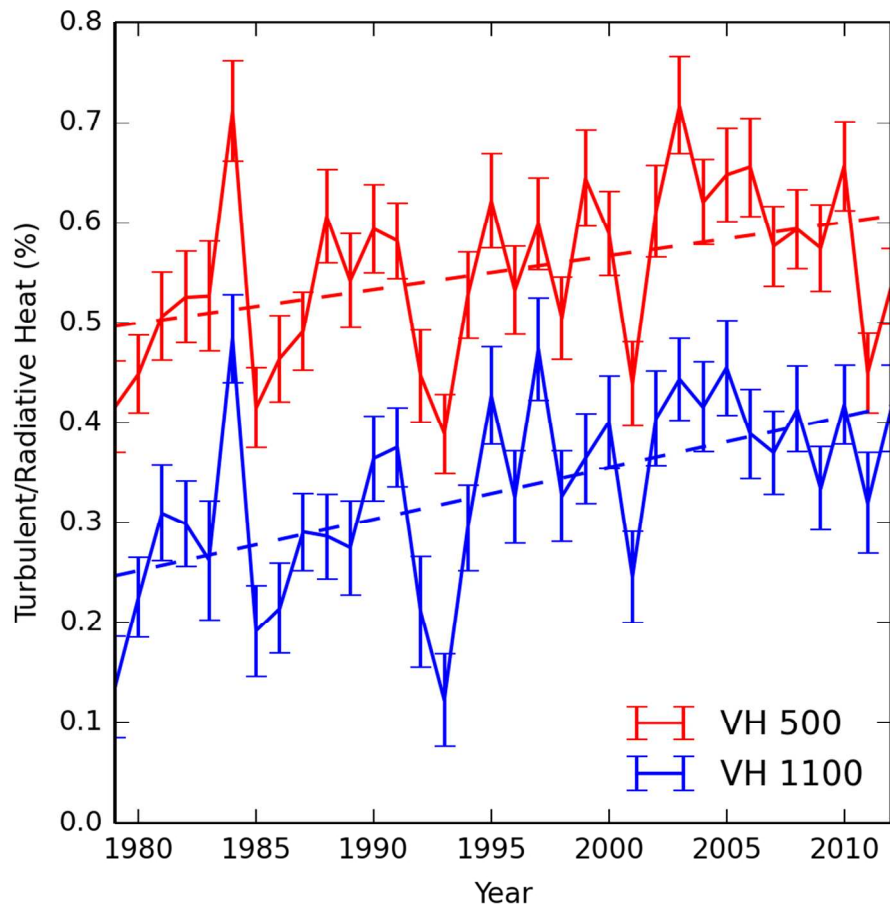
177x127mm (300 x 300 DPI)

1
2
3
4
5
6
7
8
9
10
11
12
13
14
15
16
17
18
19
20
21
22
23
24
25
26
27
28
29
30
31
32
33
34
35
36
37
38
39
40
41
42
43
44
45
46
47
48
49
50
51
52
53
54
55
56
57
58
59
60



160x120mm (300 x 300 DPI)

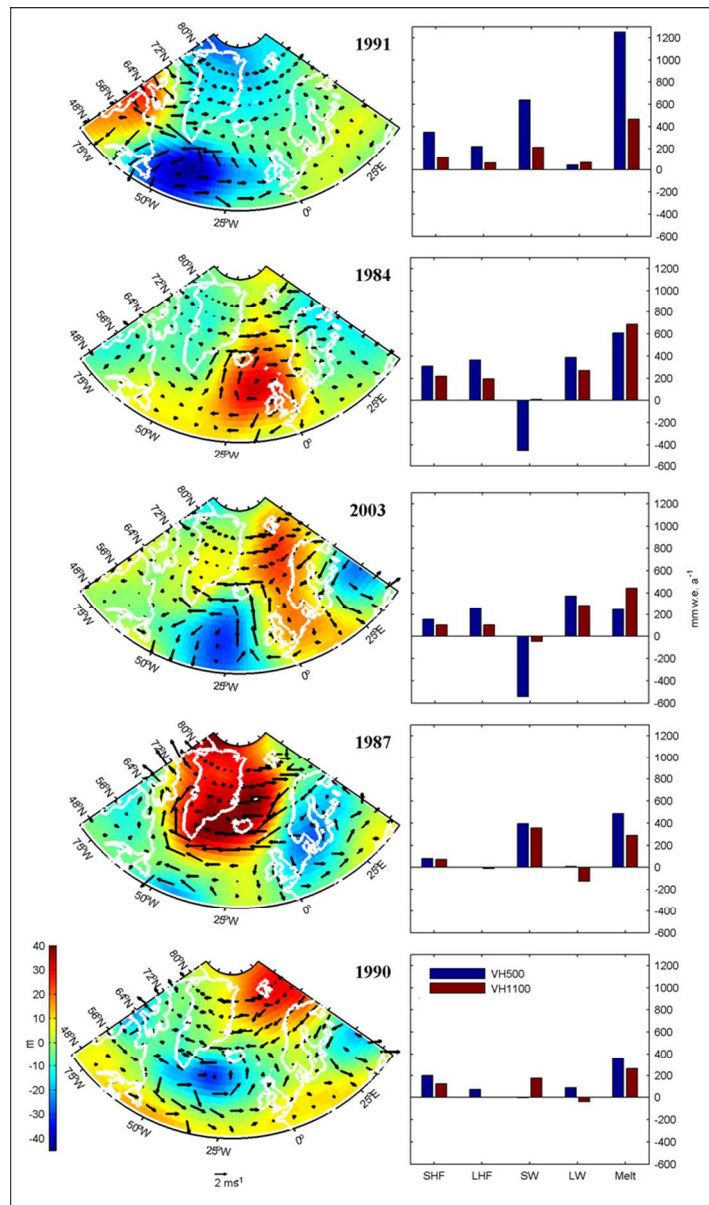
1
2
3
4
5
6
7
8
9
10
11
12
13
14
15
16
17
18
19
20
21
22
23
24
25
26
27
28
29
30
31
32
33
34
35
36
37
38
39
40
41
42
43
44
45
46
47
48
49
50
51
52
53
54
55
56
57
58
59
60



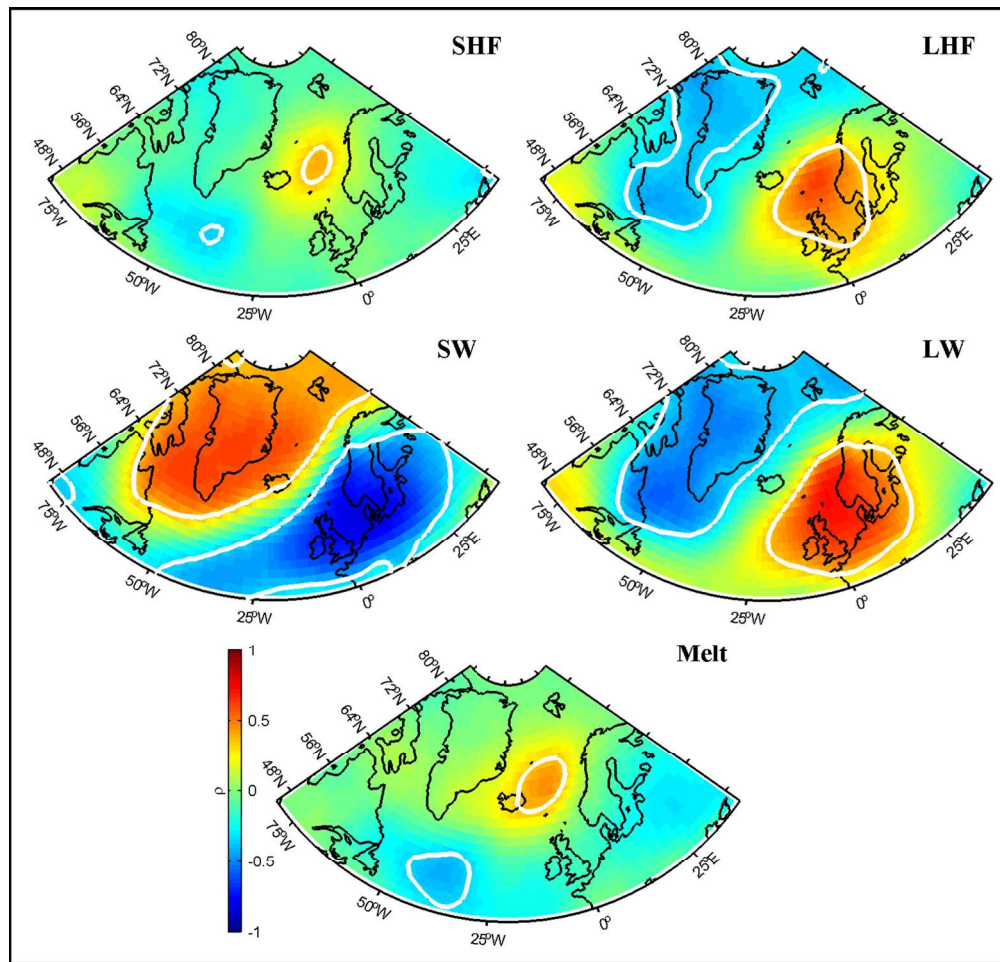
101x101mm (300 x 300 DPI)



1
2
3
4
5
6
7
8
9
10
11
12
13
14
15
16
17
18
19
20
21
22
23
24
25
26
27
28
29
30
31
32
33
34
35
36
37
38
39
40
41
42
43
44
45
46
47
48
49
50
51
52
53
54
55
56
57
58
59
60



138x234mm (150 x 150 DPI)



138x132mm (300 x 300 DPI)